Ceramics International 45 (2019) 8279–8285

Contents lists available at ScienceDirect

Ceramics International

journal homepage: www.elsevier.com/locate/ceramint

Co-doping as a strategy for tailoring the electrolyte properties of $BaCe_{0.9}Y_{0.1}O_{3-\delta}$

Aleksandar Radojković[a,*], Milan Žunić[a], Slavica M. Savić[b], Sanja Perać[a], Danijela Luković Golić[a], Zorica Branković[a], Goran Branković[a]

[a] Institute for Multidisciplinary Research, University of Belgrade, Kneza Višeslava 1a, 11030, Belgrade, Serbia
[b] University of Novi Sad, BioSense Institute, Nano and Microelectronics Group, Dr Zorana Đinđića 1, 21000, Novi Sad, Serbia

ARTICLE INFO

Keywords:
Calcination
Grain boundaries
Ionic conductivity
Perovskites
Fuel cells

ABSTRACT

The properties of single-doped $BaCe_{0.9}Y_{0.1}O_{3-\delta}$ and materials co-doped with 5 mol % of different cations (In^{3+}, Zr^{4+} and Nb^{5+}) with the general formula $BaCe_{0.85}Y_{0.1}M_{0.05}O_{3-\delta}$ were compared to examine the influence of dopants on the electrolyte properties. The samples were synthesized by the citric-nitric autocombustion method. $BaCe_{0.85}Y_{0.1}In_{0.05}O_{3-\delta}$ was successfully sintered at 1400 °C for 5 h in air, while a complete sintering of the other materials was carried out at 1550 °C. This makes the doping with In a preferable method since sintering temperatures below 1500 °C can limit BaO evaporation. The total conductivities (σ) calculated from the electrical measurements at 700 °C in wet hydrogen decreased in the following order:

$BaCe_{0.9}Y_{0.1}O_{3-\delta}$ > $BaCe_{0.85}Y_{0.1}Zr_{0.05}O_{3-\delta}$ > $BaCe_{0.85}Y_{0.1}Nb_{0.05}O_{3-\delta}$ > $BaCe_{0.85}Y_{0.1}In_{0.05}O_{3-\delta}$. The stability of the ceramics exposed to a 100% CO_2 atmosphere at 700 °C for 5 h was examined by X-ray analysis. It was observed that only $BaCe_{0.85}Y_{0.1}In_{0.05}O_{3-\delta}$ could sustain the aggressive environment containing traces of secondary phases, while the other samples were partially or significantly decomposed. By taking into account the values of the Goldschmidt tolerance factor (*t*) and dopant electronegativity (χ), it was found that the dopant electronegativity had a decisive role in inhibiting the carbonation of the ceramics.

1. Introduction

$BaCe_{0.9}Y_{0.1}O_{3-\delta}$ has been one of the most studied materials, known for its highest proton conductivity at temperatures between 500 and 700 °C, which enables its application as a proton conducting electrolyte for intermediate-temperature solid oxide fuel cells (IT-SOFC) [1]. The proton conductivity is an exclusive property of mixed oxides with a loosely packed perovskite structure and a large unit cell volume, such as $BaCeO_3$ or $SrCeO_3$ [2]. Doping with trivalent cations (Y^{3+}, In^{3+}) that replace Ce^{4+} induces a formation of point defects (oxygen vacancies), which in a wet or hydrogen-containing atmosphere enables proton mobility [1–5]. The main disadvantage of this material is its instability in a CO_2-rich atmosphere due to the basic character of the crystal lattice, thus limiting its application in SOFCs with respect to fuel selection [1–4]. However, it was found that the stability of $BaCe_{0.9}Y_{0.1}O_{3-\delta}$ was related to the Goldschmidt tolerance factor (*t*) and that it can be increased by introducing smaller doping cations [4]. The other approach implies that the stability can be enhanced by doping with cations, such as Nb^{5+}, Ta^{5+} or In^{3+} [3,6–8], that may raise the acidic character of the material. However, an introduction of pentavalent cations will lead to a reduced amount of point defects and consequently to a lower proton conductivity. It is therefore recommended that their molar concentration should be much lower than that of a trivalent cation in co-doped compositions [4]. On the other hand, trivalent In^{3+} seems more suitable as it can completely replace Y^{3+} and serve both as a point defect source and an inhibitor of the electrolyte degradation caused by CO_2 [8]. Because of these properties, it can be introduced in much larger amounts than Nb^{5+} or Ta^{5+}.

It has been found that the proton conductivity in perovskites also depends on the crystal lattice parameters (unit cell volume) and the value of the Goldschmidt tolerance factor [3,4,9]. Both a decrease of the unit cell volume and a higher degree of lattice distortion caused by doping will decrease the proton conductivity as well. In addition to this, the molar enthalpy of the formation of proton defects, expressed by the following equation:

$$H_2O(g) + V_O^{\bullet\bullet} + O_O^x \rightleftharpoons 2OH_O^{\bullet} \quad (1)$$

is sensitive to dopant electronegativity and concentration at the observed temperature [2,10,11]. It is assumed that an increase in oxide charge, which favors a proton defects formation due to stronger

* Corresponding author.
E-mail address: aleksandarrr@imsi.bg.ac.rs (A. Radojković).

https://doi.org/10.1016/j.ceramint.2019.01.134
Received 7 November 2018; Received in revised form 14 January 2019; Accepted 20 January 2019
Available online 26 January 2019

O—H—O bonds, is a consequence of introducing cations of lower electronegativity. Although the conductivity of a charged species (σ_i) is simply defined as a product of its charge (z_ie), concentration (c_i) and mobility (μ_i), it is difficult to establish a clear correlation between dopant charge, concentration, ionic radius, electronegativity on the one hand, and conductivity at a given temperature on the other. Finally, the microstructure of the ceramics is also induced by dopant nature and has a great deal of influence on the electrolyte properties as well. The grain boundaries in bulk ceramics often exhibit a blocking effect for proton transport due to the Schottky barrier height present at their core [12].

Previously, we have determined the presence of a so-called "trade-off" relationship between the conductivity and the chemical stability of Nb^{5+} and Ta^{5+} co-doped $BaCe_{0.9}Y_{0.1}O_{3-\delta}$ electrolytes [6,7], and stressed the advantage of the autocombustion synthesis method in their processing [13]. In this study, we compared $BaCe_{0.9}Y_{0.1}O_{3-\delta}$ and $BaCe_{0.85}Y_{0.1}M_{0.05}O_{3-\delta}$ (M = {In, Zr, Nb}) electrolytes by taking into consideration the dopant properties (primarily the valence, electronegativity and ionic radius) and how they influenced the microstructure, conductivity and chemical stability of doped $BaCeO_3$. Although similar compounds have been studied before separately and under different conditions [3,4], this research was done with a desire to provide a more exact comparison and describe the relationships between these properties, obtained under the same experimental conditions.

2. Material and methods

$BaCe_{0.9}Y_{0.1}O_{3-\delta}$ and $BaCe_{0.85}Y_{0.1}M_{0.05}O_{3-\delta}$ (M = {In, Zr, Nb}) powders were synthesized by the method of auto-combustion reaction. Barium(II)-nitrate (Fluka, min. 99.0%), yttrium(III)-nitrate hexahydrate (Fluka, 99.8%), cerium(III)-nitrate hexahydrate (Fluka, min. 99.0%), ammonium niobate(V)-oxalate hydrate (Aldrich, 99.99%), zirconium (IV)-acetate hydroxide (Sigma-Aldrich, min. 99%), indium(III)-nitrate pentahydrate (Aldrich, 99.99%), and citric acid monohydrate (Fluka, 99%) were used as starting chemicals in the auto-combustion synthesis described in detail elsewhere [13].

Pure phase electrolyte powders were obtained after calcination of the precursor powders at 1000 °C for 5 h in a tube oven. Dense ceramic samples were produced by uniaxial pressing of the powders at 150 MPa in a cylindrical die of 8 mm in diameter, followed by sintering for 5 h at various temperatures: 1500, 1550 and 1600 °C for the $BaCe_{0.9}Y_{0.1}O_{3-\delta}$, $BaCe_{0.85}Y_{0.1}Zr_{0.05}O_{3-\delta}$ and $BaCe_{0.85}Y_{0.1}Nb_{0.05}O_{3-\delta}$ samples, and 1400 °C for the $BaCe_{0.85}Y_{0.1}In_{0.05}O_{3-\delta}$ sample. The phase purity of both ceramic powders and sintered samples was checked by X-ray diffraction (XRD, RIGAKU®) analysis using a CuK_α radiation ($\lambda_{CuK\alpha} = 1.54178 \times 10^{-10}$ m) from 20° to 80° 2θ angle and the scanning speed of 1°/min. The surface of the sintered samples was investigated by scanning electron microscopy analysis (SEM, TESCAN Vega TS5130MM). The average grain size (AGS) and the grain size distribution of the samples were determined by analyzing the SEM images using *Image Tool* software. The relative density of the $BaCe_{0.85}Y_{0.1}In_{0.05}O_{3-\delta}$ sample sintered at 1400 °C was 94% of the theoretical value. According to the SEM and XRD analyses, the sintering temperature of 1550 °C was found to be optimal for the $BaCe_{0.9}Y_{0.1}O_{3-\delta}$, $BaCe_{0.85}Y_{0.1}Zr_{0.05}O_{3-\delta}$ and $BaCe_{0.85}Y_{0.1}Nb_{0.05}O_{3-\delta}$ samples, resulting in relative densities of 96%, 93% and 92% of the theoretical values, respectively. These samples were used for further analyses.

Electrical measurements of Pt/electrolyte/Pt cells were performed on a HIOKI 3532–50 impedance analyzer between 550 and 750 °C in a wet hydrogen atmosphere (3% vol. H_2O) provided by passing hydrogen through a gas washer filled with distilled water at the room temperature. The flow rate of the gas was set at 50 cm^3/min during the measurements by a digital mass flow controller and meter (MKS PR 4000B—F). The surface area (A) and the thickness (d) of the pellet-shaped samples were measured before applying a thin layer of Pt-paste on their surfaces. Upon drying at 100 °C for 2 h the samples were further treated at 750 °C for 30 min. The total conductivities were calculated from the resistivities (R) measured at 550, 600, 650, 700 and 750 °C ($\sigma = 1/R \times d/A$). The $BaCe_{0.85}Y_{0.1}In_{0.05}O_{3-\delta}$ sample was also analyzed at lower temperatures (150–200 °C) to examine the influence of the microstructure on the electrical properties, i.e. bulk and grain boundary contributions to the total conductivity. The activation energies were calculated from the slope values of Arrhenius plots, ln (σT)–1/T.

The stability of the electrolyte compounds was examined in the so-called accelerated degradability test, where the sintered samples were exposed to a pure CO_2 atmosphere at 700 °C for 5 h. The flow rate of CO_2 through the aperture was kept constant at 400 cm^3/min. After the exposure, the pellets were examined by XRD analysis to identify eventual changes in their composition. The content of undecomposed electrolytes was determined using *PowderCell* software.

3. Results and discussion

The autocombustion synthesis method was proved to be very yielding and reproducible, since no impurity phase was detected for all the powders calcined at 1000 °C for 5 h and subsequently for the sintered samples obtained from these powders (Fig. 1). The $BaCe_{0.85}Y_{0.1}In_{0.05}O_{3-\delta}$ sample was successfully sintered at 1400 °C for 5 h in air, while the optimal sintering condition for $BaCe_{0.9}Y_{0.1}O_{3-\delta}$, $BaCe_{0.85}Y_{0.1}Zr_{0.05}O_{3-\delta}$ and $BaCe_{0.85}Y_{0.1}Nb_{0.05}O_{3-\delta}$ to form single phased, gas-tight electrolytes was temperature treatment at 1550 °C for 5 h in air. The lower sinterability of Zr and Nb co-doped $BaCe_{0.9}Y_{0.1}O_{3-\delta}$ has already been reported in literature [3,6,7,13,14], and the sintering

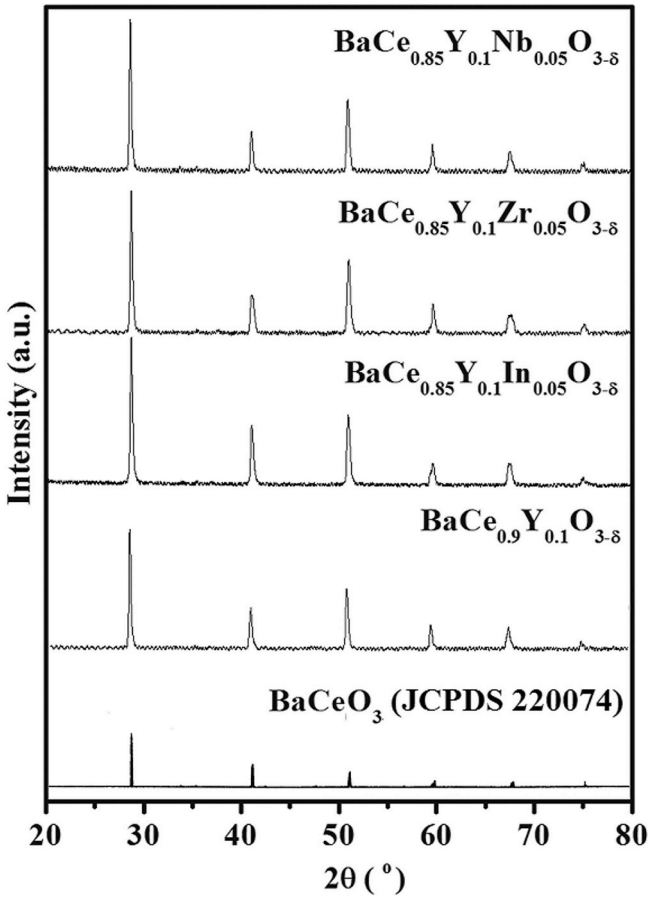

Fig. 1. XRD patterns of the ceramic samples sintered for 5 h in air at: 1550 °C ($BaCe_{0.9}Y_{0.1}O_{3-\delta}$, $BaCe_{0.85}Y_{0.1}Zr_{0.05}O_{3-\delta}$, $BaCe_{0.85}Y_{0.1}Nb_{0.05}O_{3-\delta}$ [13]) and 1400 °C ($BaCe_{0.85}Y_{0.1}In_{0.05}O_{3-\delta}$). The major reflection lines of $BaCeO_3$ (JCPDS 220074) were given as a reference.

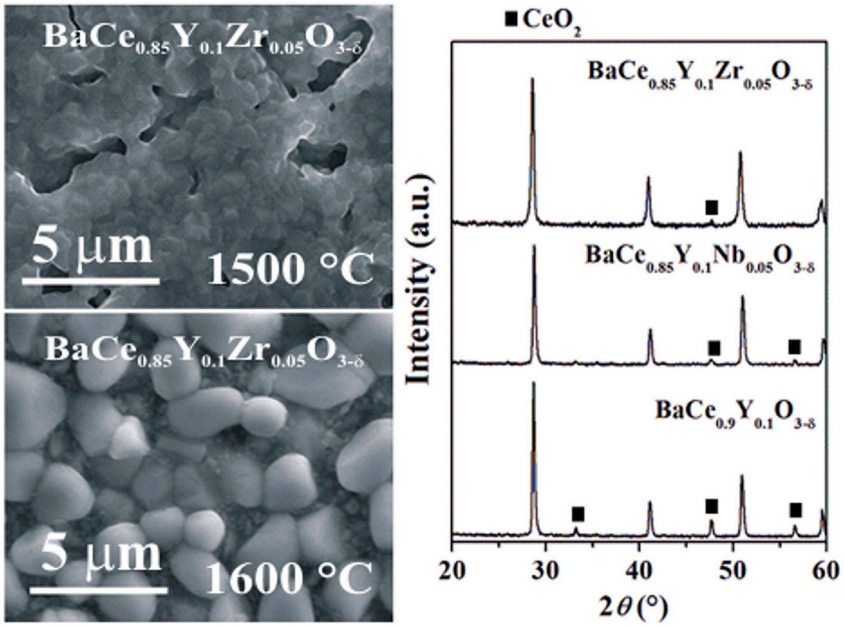

Fig. 2. SEM images of the $BaCe_{0.85}Y_{0.1}Zr_{0.05}O_{3-\delta}$ microstructure obtained at 1500 and 1600 °C and XRD analysis of the $BaCe_{0.9}Y_{0.1}O_{3-\delta}$, $BaCe_{0.85}Y_{0.1}Nb_{0.05}O_{3-\delta}$ and $BaCe_{0.85}Y_{0.1}Zr_{0.05}O_{3-\delta}$ samples sintered at 1600 °C.

temperatures near 1500 °C were not enough to avoid open porosity. On the other hand, a certain decomposition of the samples occurred at 1600 °C as presented in Fig. 2. The peaks of CeO_2 as the only secondary phase indicate that the material becomes Ba-deficient at higher temperatures according to the following equation:

$$BaCe_{1-x}M_xO_{3-\delta}(s) \xrightarrow{>1500\ ^\circ C} BaO\uparrow + Ce_{1-x}M_xO_{2-\delta}(s) \quad (2)$$

where M = {Y, In, Zr, Nb} and combinations thereof. Although the decomposition of $BaCe_{0.85}Y_{0.1}Zr_{0.05}O_{3-\delta}$ was negligible, an abnormal grain growth in this sample was observed after sintering at 1600 °C (Fig. 2). Therefore, the samples sintered at 1500 and 1600 °C were not further investigated. This implies that a very narrow temperature range is left for successful sintering of the $BaCe_{0.9}Y_{0.1}O_{3-\delta}$ and Zr and Nb co-doped samples. On the other hand, the presence of In provides good sinterability of $BaCe_{0.9}Y_{0.1}O_{3-\delta}$ at lower temperatures [15–17].

The structural stability of the samples was discussed in terms of the value of the Goldschmidt tolerance factor. In the case of a system defined as $BaCe_{0.85}M_{0.05}Y_{0.1}O_{3-\delta}$, where M = {$In^{3+}$, Zr^{4+}, Nb^{5+}}, the Goldschmidt tolerance factor is calculated using the following formula [4]:

$$t = \frac{rBa_{XII}^{2+} + rO_{VI}^{2-}}{\sqrt{2}\,[0.85 \cdot rCe_{VI}^{4+} + 0.05 \cdot rM_{VI} + 0.1 \cdot rY_{VI}^{3+} + rO_{VI}^{2-}]} \quad (3)$$

where *r* denotes the radius of the ions, while the Roman numerals in the subscript represent their coordination number. An increase in the Goldschmidt tolerance factor value leads to the stabilization of the perovskite structure, according to the literature [4,9]. It was found that the values slightly decreased in the following order: $BaCe_{0.85}Y_{0.1}Nb_{0.05}O_{3-\delta}$ > $BaCe_{0.85}Y_{0.1}Zr_{0.05}O_{3-\delta}$ > $BaCe_{0.85}Y_{0.1}In_{0.05}O_{3-\delta}$ > $BaCe_{0.9}Y_{0.1}O_{3-\delta}$, as it was shown in Table 1. The most stable structure according to this criterion is that of $BaCe_{0.85}Y_{0.1}Nb_{0.05}O_{3-\delta}$, which led to the conclusion that $BaCe_{0.9}Y_{0.1}O_{3-\delta}$ could be stabilized with an introduction of smaller cations. This trend was not straightforward when it comes to the total conductivity values measured in the wet hydrogen atmosphere at 700 °C (Table 1).

3.1. Conductivity of the electrolytes

Although $BaCe_{0.9}Y_{0.1}O_{3-\delta}$ -based electrolytes have been known as good proton conductors, these compounds belong to a class of mixed ionic (both proton and oxygen ion) conductors as it is implied by Equation (1). Thus, it is more appropriate to speak of total conductivity than of proton conductivity despite the fact that the latter was shown to be dominant in wet and hydrogen containing atmospheres in the temperature interval between 500 °C and 700 °C [18,19]. For clarity reasons, it is convenient to point out the major factors and discuss their influence on the electrolyte conductivities.

1) Concentration of point defects (oxygen vacancies/protons)

Incorporation of aliovalent dopants can be described by the following equations using the Kröger-Vink notation:

$$Ce_{Ce}^{x} + \frac{1}{2}O_O^x + \frac{1}{2}M_2O_3(s) \rightarrow M_{Ce}^{'} + \frac{1}{2}V_O^{\cdot\cdot} + CeO_2(s)\ (\text{trivalent dopants: } In^{3+}, Y^{3+}) \quad (4)$$

$$Ce_{Ce}^{x} + \frac{1}{2}MO_2(s) \rightarrow M_{Ce}^{x} + CeO_2(s)\ (\text{tetravalent dopants: } Zr^{4+}) \quad (5)$$

$$Ce_{Ce}^{x} + \frac{1}{2}V_O^{\cdot\cdot} + \frac{1}{2}M_2O_5(s) \rightarrow M_{Ce}^{\cdot} + \frac{1}{2}O_O^x + CeO_2(s)\ (\text{pentavalent dopants: } Nb^{5+}) \quad (6)$$

It is obvious that the dopant valence and concentration govern the formation and abundance of oxygen vacancies (Equations (4)–(6)), which in wet or hydrogen containing atmospheres can be protonated allowing proton mobility through the perovskite structure at elevated temperatures (Equation (1)). Given that the other parameters are constant, the conductivity is directly proportional to the concentration of oxygen ion vacancies/proton defects:

$$\sigma^{total} = \sum_i \sigma^i = \sum_i z_i e c_i \mu_i \quad (7)$$

where σ_i represents partial conductivity, $z_i e$ charge, c_i concentration and μ_i mobility of the of the species *i*. The highest conductivity is observed for $BaCe_{0.9}Y_{0.1}O_{3-\delta}$, although according to Equations (4)–(6) the highest total theoretical amount of oxygen vacancies can be obtained in

Table 1
Properties of the $BaCe_{0.9}Y_{0.1}O_{3-\delta}$-based samples as a function of dopant nature.

Sample	Average grain size, (μm)	Electronegativity, χ[a] (a.u.)	Ionic radius, r[b] (pm)	Goldschmidt tolerance factor, t (a.u)	Total conductivity in wet H_2 at 700 °C, σ ($\times 10^{-2}$ S/cm)
$BaCe_{0.9}Y_{0.1}O_{3-\delta}$	1.5	1.22 (Y)	90 (Y^{3+})	0.938	1.34 this study
$BaCe_{0.85}Y_{0.1}In_{0.05}O_{3-\delta}$	1.0	1.78 (In)	80 (In^{3+})	0.941	0.48 this study
$BaCe_{0.85}Y_{0.1}Zr_{0.05}O_{3-\delta}$	1.2	1.33 (Zr)	72 (Zr^{4+})	0.942	1.00 this study
$BaCe_{0.85}Y_{0.1}Nb_{0.05}O_{3-\delta}$	1.3	1.60 (Nb)	64 (Nb^{5+})	0.944	0.54 [13]

[a] $\chi(Ce) = 1.12$; $\chi(Ba) = 0.89$; $\chi(O) = 3.44$.
[b] $r_{VI}(Ce^{4+}) = 87$ p.m.; $r_{XII}(Ba^{2+}) = 161$ p.m.; $r_{VI}(O^{2-}) = 140$ p.m.

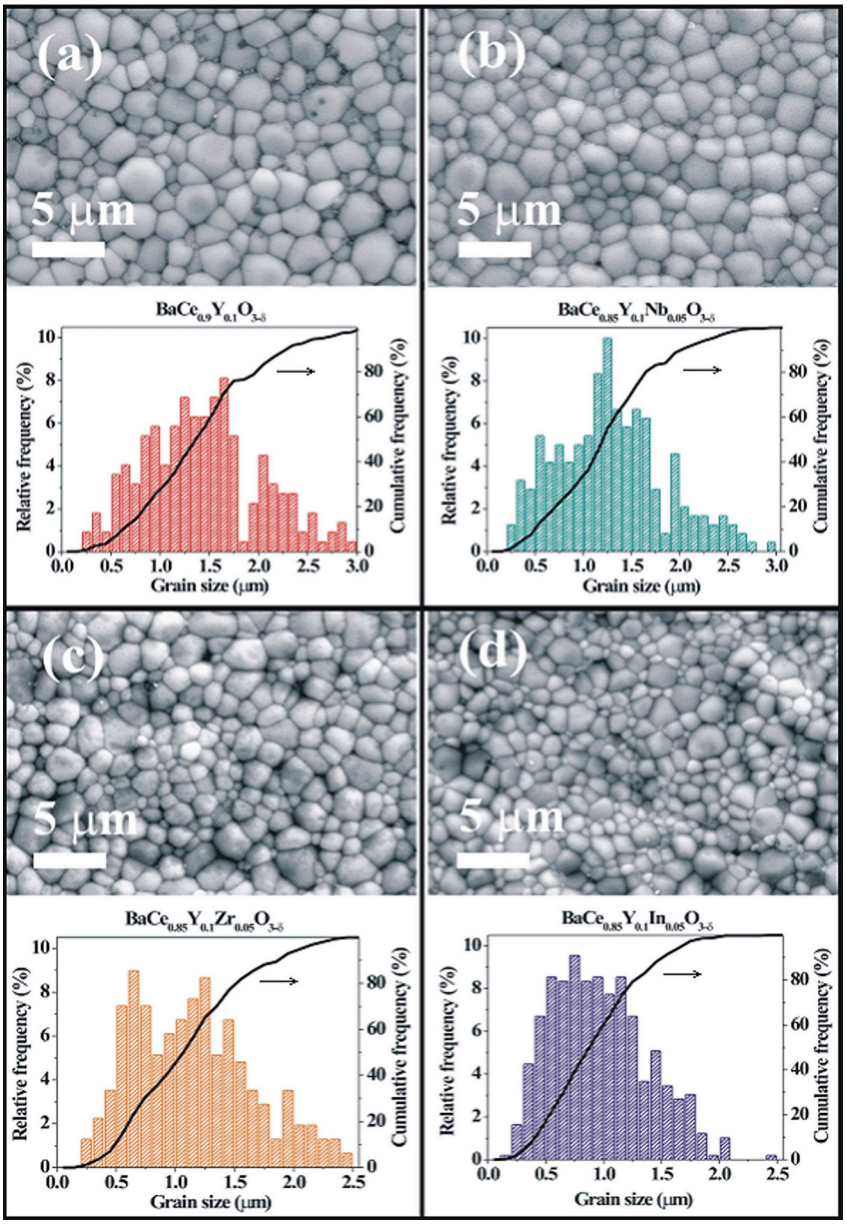

Fig. 3. Grain size distribution histograms and SEM images of the surface of the sintered samples: a) $BaCe_{0.9}Y_{0.1}O_{3-\delta}$, b) $BaCe_{0.85}Y_{0.1}Nb_{0.05}O_{3-\delta}$, c) $BaCe_{0.85}Y_{0.1}Zr_{0.05}O_{3-\delta}$ and d) $BaCe_{0.85}Y_{0.1}In_{0.05}O_{3-\delta}$.

$BaCe_{0.85}Y_{0.1}In_{0.05}O_{3-\delta}$ (7.5 mol %). By comparison, it is 5 mol % for $BaCe_{0.9}Y_{0.1}O_{3-\delta}$ and $BaCe_{0.85}Y_{0.1}Zr_{0.05}O_{3-\delta}$, and 2.5 mol % for $BaCe_{0.85}Y_{0.1}Nb_{0.05}O_{3-\delta}$, which exhibited the second lowest conductivity in the wet hydrogen atmosphere at 700 °C (Table 1). The lowest conductivity of $BaCe_{0.85}Y_{0.1}In_{0.05}O_{3-\delta}$ apparently indicates a lower mobility of the charge carriers in this compound at a given temperature. Besides, the difference in the conductivities between $BaCe_{0.9}Y_{0.1}O_{3-\delta}$ and $BaCe_{0.85}Y_{0.1}Zr_{0.05}O_{3-\delta}$, both of which contain the same level of acceptor doping, is not negligible. These findings imply that: a) the equilibrium state defined by Equation (1) is different for various dopants resulting in a different distribution of the charge carries' concentration at a given temperature; b) the dopants change the structural

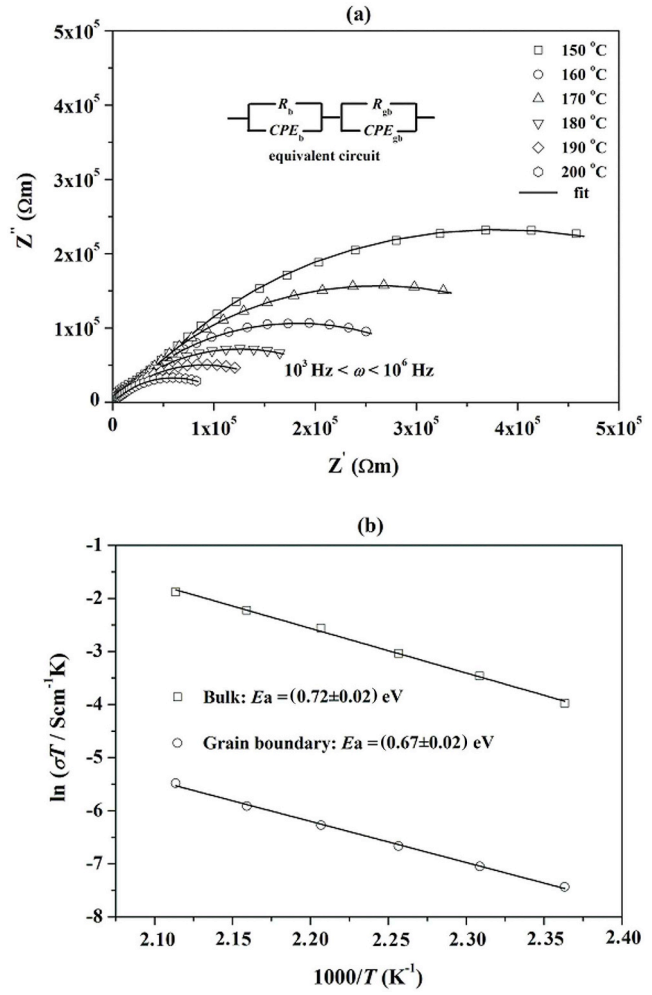

Fig. 4. Conductivities of $BaCe_{0.85}Y_{0.1}In_{0.05}O_{3-\delta}$ measured at 150–200 °C in wet hydrogen presented in the form of Nyquist plots (a) and activation energies for the bulk and the grain boundary conduction calculated from the Arrhenius plots (b).

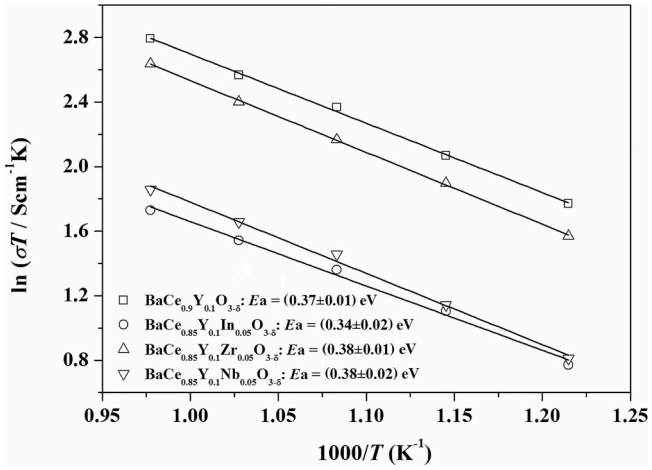

Fig. 5. Total conductivities presented in the form of Arrhenius plots measured at 550–750 °C in wet hydrogen.

and chemical environment of $BaCe_{0.9}Y_{0.1}O_{3-\delta}$ affecting the mobility and the conduction mechanism of the charge carriers. Both assumptions are crucial for understanding the unexpectedly low total conductivity of $BaCe_{0.85}Y_{0.1}In_{0.05}O_{3-\delta}$.

2) Dopant nature: electronegativity, ionic radius and charge

Although the formation of the proton defects (Equation (1)) is an exothermic process ($\Delta_r H < 0$), Norby et al. [10,11] suggested that the enthalpy of this reaction depended on the electronegativity of dopants expressed by the following empirical equation:

$$\Delta_r H = -173(9) + 370(42)\Delta\chi_{B-A} \quad (8)$$

where $\Delta\chi_{B-A}$ represents the difference in electronegativity between the cations A and B of the perovskite compounds described by the general formula ABO_3. With an introduction of more electronegative cations (In^{3+}, Nb^{5+}), the reaction described by Equation (1) becomes less exothermic, and the maximal concentration of proton defects should be shifted towards higher temperatures in the case of more electronegative dopants. This behavior was confirmed previously by comparing the conductivity values for $BaCe_{0.9-x}Nb_xY_{0.1}O_{3-\delta}$ obtained in dry argon (no proton conductivity) and wet hydrogen (mixed conductivity) atmospheres at different temperatures and for various Nb concentrations [6]. In general, it is assumed that the basicity of the oxygen ion is important in the conduction mechanism of protons, and that more electronegative cations can suppress the oxygen dynamics responsible for high proton mobility at operating temperatures [2,4]. Although the addition of In increases the concentration of point defects in $BaCe_{0.9}Y_{0.1}O_{3-\delta}$ (Equation (4)), its relatively high electronegativity ($\chi = 1.78$) disables the oxygen ions in its vicinity to take part in the proton conducting mechanism. This is also the case with co-doping with somewhat less electronegative Nb ($\chi = 1.60$), for its addition to $BaCe_{0.9}Y_{0.1}O_{3-\delta}$ decreases the concentration of the point defects according to Equation (6). Furthermore, the drop in the total conductivity of the $BaCe_{0.85}Y_{0.1}Zr_{0.05}O_{3-\delta}$ ($\sigma = 1.00 \times 10^{-2}$ S/cm) as compared with $BaCe_{0.9}Y_{0.1}O_{3-\delta}$ ($\sigma = 1.34 \times 10^{-2}$ S/cm) can be explained by the introduction of the more electronegative element Zr ($\chi = 1.33$) in the place of Ce ($\chi = 1.12$), particularly when the level of acceptor doping remains unchanged as described by Equation (5).

It was reported that the ionic radius of a doping cation at the B-site of the perovskite structure (ABO_3) plays important role in the proton conducting mechanism [4,9,20]. Decrease of the unit cell volume and deformation of the crystal lattice caused by doping with smaller cations will lead to higher packing densities with a reduced water solubility limit [2,4]. It can be accompanied by a deformation of octahedrons, whereby the oxygen ions may occupy chemically inequivalent sites characterized by different bond lengths between them and the central cation [2], in this case Y^{3+}, In^{3+}, Zr^{4+}, Ce^{4+} or Nb^{5+}. According to the radii size presented in Table 1, one should expect a monotonous decrease of the total conductivities in the following sequence: $BaCe_{0.9}Y_{0.1}O_{3-\delta}$ > $BaCe_{0.85}Y_{0.1}In_{0.05}O_{3-\delta}$ > $BaCe_{0.85}Y_{0.1}Zr_{0.05}O_{3-\delta}$ > $BaCe_{0.85}Y_{0.1}Nb_{0.05}O_{3-\delta}$, but the unexpectedly lower conductivity of $BaCe_{0.85}Y_{0.1}In_{0.05}O_{3-\delta}$ suggests that the ionic radius by itself has no decisive impact on the proton conductivity. Furthermore, the higher the charge of a dopant, the stronger will be the electrostatic repulsion between protons and dopant cations, which can also have a negative effect on the proton conductivity. Again, this assumption is not valid in the case of the $BaCe_{0.85}Y_{0.1}In_{0.05}O_{3-\delta}$ electrolyte, i.e. when it comes to the dopant properties, the electronegativity can be considered as the key factor with the highest impact on the proton conductivity and total conductivity, consequently. Moreover, the charge/valence of the dopant is much more important for the concentration of the defects, as discussed in the previous paragraph.

3) Microstructure

The average grain size plays important role when it comes to the proton conductivity and ionic conductivity in general. Grain boundaries in this type of materials have been known for their insulating effect due to the presence of the Shottky barrier height at their core [10,12,21]. According to the SEM images of the surfaces of the electrolyte samples

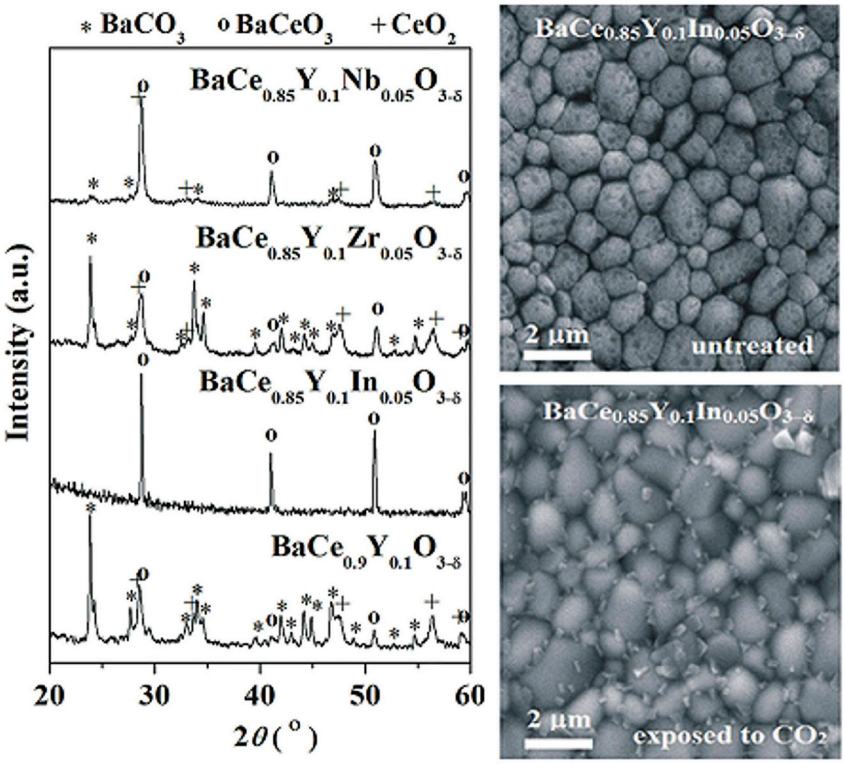

Fig. 6. XRD analysis of the sintered electrolyte samples after exposure to 100% CO_2 atmosphere for 5 h and SEM analysis of the $BaCe_{0.85}Y_{0.1}In_{0.05}O_{3-\delta}$ sample before and after exposure to CO_2.

presented in Fig. 3 and the AGS values given in Table 1, the low conductivity of $BaCe_{0.85}Y_{0.1}In_{0.05}O_{3-\delta}$ can be attributed to the microstructure as well. All the samples have a similar microstructural pattern and the AGS decreases in the following sequence:

$BaCe_{0.9}Y_{0.1}O_{3-\delta}$ > $BaCe_{0.85}Y_{0.1}Nb_{0.05}O_{3-\delta}$ > $BaCe_{0.85}Y_{0.1}Zr_{0.05}O_{3-\delta}$ > $BaCe_{0.85}Y_{0.1}In_{0.05}O_{3-\delta}$.

The grain size distribution for each sample was presented in the form of a histogram (Fig. 3). It became narrower as the AGS decreased and the transition from a bimodal to a unimodal grain size distribution was observed for $BaCe_{0.85}Y_{0.1}In_{0.05}O_{3-\delta}$. This decrease in the AGS for the Nb and Zr co-doped $BaCe_{0.9}Y_{0.1}O_{3-\delta}$ can be explained by the lower sinterability of these materials as it was mentioned earlier. In the case of $BaCe_{0.85}Y_{0.1}In_{0.05}O_{3-\delta}$, the narrower grain size distribution and the lowest AGS value are a consequence of the relatively low sintering temperature.

At temperatures above 500 °C it is usually hard to determine and separate the contributions of the bulk and the grain boundaries by electrochemical impedance spectroscopy analysis. Therefore, to study the influence of the microstructure on the electrical properties, low temperature measurements were performed for the sample $BaCe_{0.85}Y_{0.1}In_{0.05}O_{3-\delta}$. The impedance spectra measured from 150 to 200 °C in the form of Nyquist plots were shown in Fig. 4a. The fitting of the characteristic semicircles was carried out using *EIS Spectrum Analyzer* software in the high and medium frequency range (10^6 Hz > ω > 10^3 Hz) to avoid the influence of electrode processes on the fit accuracy. The equivalent circuit consisted of two resistors, R_b and R_{gb}, and two constant phase elements, CPE_b and CPE_{gb}, where the subscripts "b" and "gb" denote the bulk and the grain boundary, respectively. The impedance curves consisted of two overlapping semicircles, whereby the contribution of the bulk and the grain boundaries to the total conductivity was calculated and presented in Fig. 4b. It was found that the grain boundary resistivity was almost 4 orders of magnitude higher than the bulk resistivity. These results suggest that a higher abundance of grain boundaries per unit of volume will increase the resistivity of the electrolyte, and even at higher temperatures one may expect their contribution to the total resistivity.

4) Temperature

The formation of the proton defects becomes favorable at temperatures above 400 °C (although $\Delta_r H < 0$), while at the same time the proton conductivity is a type of ionic conductivity and increases with temperature. Therefore, it is typical for the proton conductivity to reach the maximum value at some point after which it declines with a further increase in temperature. Activation energies calculated from the temperature dependence of the total conductivities measured at 550–750 °C in wet hydrogen were presented in Fig. 5. The values around 0.4 eV are typical for the proton conduction of doped $BaCeO_3$ at observed temperatures [2,5–9]. At lower temperatures (150–200 °C), the total conductivity of $BaCe_{0.85}Y_{0.1}In_{0.05}O_{3-\delta}$ dropped about 2 orders of magnitude, while the activation energy increased to ~0.7 eV, which is characteristic for oxygen ion conductivity. This means that at lower temperatures the proton defects (Equation (1)) cannot be formed and thus are not involved in the conducting mechanism.

3.2. Stability of the electrolytes

The stability of the sintered electrolyte samples was determined by XRD analysis after their exposure to a 100% CO_2 atmosphere at 700 °C for 5 h (Fig. 6). It was found that the stability trend was quite opposite to the proton conductivity trend observed at 550–750 °C. Although no peaks of the carbonate phase were found in the $BaCe_{0.85}Y_{0.1}In_{0.05}O_{3-\delta}$ sample, SEM analysis revealed a slight deterioration of its microstructure, whereby small crystallites of the secondary phase were formed during the exposure to CO_2, as presented in Fig. 6. The

degradation mechanism of $BaCeO_3$–based materials can be described by the following equation:

$$BaCeO_3(s) + CO_2(g) \overset{t}{\Leftrightarrow} BaCO_3(s) + CeO_2(s) \quad (9)$$

If we extract the Goldschmidt tolerance factor and dopant electronegativity as the key parameters for the structural stability of the selected electrolytes in an acidic environment, it becomes obvious that the dopant electronegativity plays a dominant role in inhibiting the deterioration of the electrolyte structure. The Nb co-doped sample also showed a sufficient stability (91 mass % of the undecomposed phase), keeping in mind a very aggressive environment simulating a sort of an accelerated stability test. Although its structure possesses a slightly higher t value (0.944) than $BaCe_{0.85}Y_{0.1}In_{0.05}O_{3-\delta}$ (0.941), it is outbalanced by a significant difference in electronegativity ($\chi_{Nb} = 1.60$, $\chi_{In} = 1.78$). Even though both the electronegativity of Zr ($\chi_{Zr} = 1.33$) and the t value of $BaCe_{0.85}Y_{0.1}Zr_{0.05}O_{3-\delta}$ (0.942) favored the improvement in terms of stability, 5 mol% of Zr was not enough to suppress the degradation of the electrolyte under the same conditions. Thus, the mass content of the undecomposed electrolyte after the exposure to CO_2 slightly increased from 26% for $BaCe_{0.9}Y_{0.1}O_{3-\delta}$ to 31% in the case of $BaCe_{0.85}Y_{0.1}Zr_{0.05}O_{3-\delta}$.

4. Conclusions

In this study, dopants of different properties were used to examine the key parameters that influence the proton conductivity and the structure stability of $BaCe_{0.9}Y_{0.1}O_{3-\delta}$-based materials. It was found that dopant electronegativity exerted decisive but opposite effects: negative on the proton conductivity and positive on the chemical stability of doped $BaCe_{0.9}Y_{0.1}O_{3-\delta}$. Thus, In and Nb co-doped $BaCe_{0.9}Y_{0.1}O_{3-\delta}$ scored the lowest total conductivity between 550 and 750 °C in the wet hydrogen atmosphere and were highly stable in the 100% CO_2 atmosphere at 700 °C for 5 h. On the other hand, 5 mol % of Zr was insufficient to inhibit the degradation of the electrolyte. The slight differences in the t values (0.938–0.944) suggested that structural changes induced by 5 mol % co-doping were insignificant to have a stronger impact on the electrolyte stability in the CO_2 atmosphere. The acceptor doping mechanism enables In^{3+} to be present at higher concentrations in $BaCe_{0.9}Y_{0.1}O_{3-\delta}$ than Nb^{5+} or other pentavalent cation. In^{3+} can even completely replace Y^{3+} in $BaCe_{0.9}Y_{0.1}O_{3-\delta}$. In addition to this, In^{3+} promotes sinterability at lower temperatures (~1400 °C), which facilitates the processing of the ceramics to form a functional electrolyte for SOFCs. This all makes the co-doping with In more advantageous than the co-doping with Nb or Zr.

Acknowledgements

The authors acknowledge that the Ministry of Education, Science and Technological Development of the Republic of Serbia [project number III45007] supported this work.

References

[1] G. Ma, T. Shimura, H. Iwahara, Ionic conduction and nonstoichiometry in $Ba_xCe_{0.90}Y_{0.10}O_{3-\alpha}$, Solid State Ionics 110 (1998) 103–110 https://doi.org/10.1016/S0167-2738(98)00130-1.

[2] K.D. Kreuer, On the development of proton conducting materials for technological applications, Solid State Ionics 97 (1997) 1–15 https://doi.org/10.1016/S0167-2738(97)00082-9.

[3] D. Medvedev, A. Murashkina, E. Pikalova, A. Demin, A. Podias, P. Tsiakaras, $BaCeO_3$: materials development, properties and application, Prog. Mater. Sci. 60 (2014) 72–129 https://doi.org/10.1016/j.pmatsci.2013.08.001.

[4] D.A. Medvedev, J.G. Lyagaeva, E.V. Gorbova, A.K. Demin, P. Tsiakaras, Advanced materials for SOFC application: strategies for the development of highly conductive and stable solid oxide proton electrolytes, Prog. Mater. Sci. 75 (2016) 38–79 https://doi.org/10.1016/j.pmatsci.2015.08.001.

[5] W. Münch, K.D. Kreuer, St Adams, G. Seifert, J. Maier, The relation between crystal structure and the formation and mobility of protonic charge carriers in perovskite-type oxides: a case study of Y-doped $BaCeO_3$ and $SrCeO_3$, Phase Transitions 68/3 (1999) 567–586 https://doi.org/10.1080/01411599908224535.

[6] A. Radojković, M. Žunić, S.M. Savić, G. Branković, Z. Branković, Chemical stability and electrical properties of Nb doped $BaCe_{0.9}Y_{0.1}O_{3-\delta}$ as a high temperature proton conducting electrolyte for IT-SOFC, Ceram. Int. 39 (2013) 307–313 https://doi.org/10.1016/j.ceramint.2012.06.026.

[7] A. Radojković, M. Žunić, S.M. Savić, G. Branković, Z. Branković, Enhanced stability in CO_2 of Ta doped $BaCe_{0.9}Y_{0.1}O_{3-\delta}$ electrolyte for intermediate temperature SOFCs, Ceram. Int. 39 (2013) 2631–2637 https://doi.org/10.1016/j.ceramint.2012.09.028.

[8] L. Bi, E. Fabbri, Z. Sun, E. Traversa, Sinteractivity, proton conductivity and chemical stability of $BaZr_{0.7}In_{0.3}O_{3-\delta}$ for solid oxide fuel cells (SOFCs), Solid State Ionics 196 (2011) 59–64 https://doi.org/10.1016/j.ssi.2011.06.014.

[9] M. Amsia, D. Marrero-López, J.C. Ruiz-Morales, S.N. Savvin, M. Gabás, P. Núnez, Influence of rare-earth doping on the microstructure and conductivity of $BaCe_{0.9}Ln_{0.1}O_{3-\delta}$ proton conductors, J. Power Sources 196 (2011) 3461–3469 https://doi.org/10.1016/j.jpowsour.2010.11.120.

[10] T. Norby, Proton conductivity in perovskite oxides, in: T. Ishihara (Ed.), Perovskite Oxide for Solid Oxide Fuel Cells, Springer, Dordrecht, Heidelberg, London, New York, 2009, pp. 217–238.

[11] C. Kjølseth, L.-Y. Wang, R. Haugsrud, T. Norby, Determination of the enthalpy of hydration of oxygen vacancies in Y-doped $BaZrO_3$ and $BaCeO_3$ by TG-DSC, Solid State Ionics 181 (2010) 1740–1745 https://doi.org/10.1016/j.ssi.2010.10.005.

[12] C. Kjølseth, H. Fjeld, Ø. Prytz, P.I. Dahl, C. Estournès, R. Haugsrud, T. Norby, Space-charge theory applied to the grain boundary impedance of proton conducting $BaZr_{0.9}Y_{0.1}O_{3-\delta}$, Solid State Ionics 181 (2010) 268–275 https://doi.org/10.1016/j.ssi.2010.01.014.

[13] A. Radojković, S.M. Savić, S. Pršić, Z. Branković, G. Branković, Improved electrical properties of Nb doped $BaCe_{0.9}Y_{0.1}O_{2.95}$ electrolyte for intermediate temperature SOFCs obtained by autocombustion method, J. Alloy. Comp. 583 (2014) 278–284 https://doi.org/10.1016/j.jallcom.2013.08.189.

[14] M. Zunic, G. Brankovic, F. Basoli, M. Cilense, E. Longo, J.A. Varela, Stability, characterization and functionality of proton conducting $NiO–BaCe_{0.85-x}Nb_xY_{0.15}O_{3-\delta}$ cermet anodes for IT-SOFC application, J. Alloy. Comp. 609 (2014) 7–13 https://doi.org/10.1016/j.jallcom.2014.04.175.

[15] M. Zunic, G. Brankovic, C.R. Foschini, M. Cilense, E. Longo, J.A. Varela, Influence of the indium concentration on microstructural and electrical properties of proton conducting $NiO–BaCe_{0.9-x}In_xY_{0.1}O_{3-\delta}$ cermet anodes for IT-SOFC application, J. Alloy. Comp. 563 (2013) 254–260 https://doi.org/10.1016/j.jallcom.2013.02.122.

[16] Z. Zhang, L. Chen, Q. Li, T. Song, J. Su, B. Cai, H. He, High performance In, Ta and Y-doped $BaCeO_3$ electrolyte membrane for proton-conducting solid oxide fuel cells, Solid State Ionics 323 (2018) 25–31 https://doi.org/10.1016/j.ssi.2018.04.021.

[17] F. Zhao, Q. Liu, S. Wang, K. Brinkman, F. Chen, Synthesis and characterization of $BaIn_{0.3-x}Y_xCe_{0.7}O_{3-\delta}$ (x = 0, 0.1, 0.2, 0.3) proton conductors, Int. J. Hydrogen Energy 35 (2010) 4258–4263 https://doi.org/10.1016/j.ijhydene.2010.02.080.

[18] H. Matsumoto, Proton conduction in cerium- and zirconium-based perovskite oxides, in: T. Ishihara (Ed.), Perovskite Oxide for Solid Oxide Fuel Cells, Springer, Dordrecht, Heidelberg, London, New York, 2009, pp. 243–259.

[19] T. Norby, Solid-state protonic conductors: principles, properties, progress and prospects, Solid State Ionics 125 (1999) 1–11 https://doi.org/10.1016/S0167-2738(99)00152-6.

[20] M. Amsif, D. Marrero-López, J.C. Ruiz-Morales, S.N. Savvin, P. Núnez, Effect of sintering aids on the conductivity of $BaCe_{0.9}Ln_{0.1}O_{3-\delta}$, J. Power Sources 196 (2011) 9154–9163 https://doi.org/10.1016/j.jpowsour.2011.06.086.

[21] X. Guo, R. Waser, Space charge concept for acceptor-doped zirconia and ceria and experimental evidences, Solid State Ionics 173 (2004) 63–67 https://doi.org/10.1016/j.ssi.2004.07.053.